Itaconic acid-based 3D printed nanocomposites: An in-depth study on the effect of nanoinclusions on the physicochemical properties and the printability of formulations based

Giant, 18, 2024, 100275

Itaconic acid-based 3D printed nanocomposites: An in-depth study on the effect of nanoinclusions on the physicochemical properties and the printability of formulations based on polyester itaconates

Full-length article

Lazaros Papadopoulos[a], **Lorenzo Pezzana**[b], **Natalia Malitowski**[c], **Nikolaos Kladovasilakis**[d], **Dimitrios Tzetzis**[d], **Marco Sangermano**[b], **Dimitrios N. Bikiaris**[a,*], **Tobias Robert**[c,*]

[a] Department of Chemistry, Laboratory of Polymer Chemistry and Technology, Aristotle University of Thessaloniki, Thessaloniki GR-541 24, Greece
[b] Dipartimento Scienza Applicata e Tecnologia, Politecnico di Torino, C.so Duca degli Abruzzi 24, Torino 10129, Italy
[c] Fraunhofer Institute for Wood Research – Wilhelm-Klauditz-Institut WKI, Riedenkamp 3, Braunschweig 38108, Germany
[d] Digital Manufacturing and Materials Characterization Laboratory, International Hellenic University, School of Science and Technology, Thermi, Thessaloniki 57001, Greece

Keywords: Itaconic acid, Nanocomposites, Bio-based polymers, UV-curing, Additive manufacturing

The demand for novel bio-based materials in UV-curing additive manufacturing has surged due to increasing environmental concerns and a growing emphasis on sustainable practices in the manufacturing industry. However, at the moment, their thermomechanical performance is not equal to that of their fossil-based counterparts and this impedes the acceptance of these materials within the industrial community. Therefore, in this study, a series of nanocomposite polyesters based on itaconic acid was synthesized for the first time with *in-situ* polymerization, in an attempt to leverage the unique properties of nanofillers and improve the overall performance of the material. A variety of reinforcing agents were utilized, namely cellulose nanocrystals (CNC), montmorillonite (MMT), graphene nanoplatelets (GNP) and titanium dioxide (TiO_2), to understand the effect of each filler on the physicochemical properties of the polyester. Formulations of these polyesters were then prepared

* Corresponding authors.
E-mail addresses: dbic@chem.auth.gr (D.N. Bikiaris), tobias.robert@wki.fraunhofer.de (T. Robert).
Received 28 February 2024; Received in revised form 17 April 2024; Accepted 23 April 2024

 https://doi.org/10.1016/j.giant.2024.100275

and processed on a digital light processing (DLP) 3D printer to prepare test specimens. Extensive thermomechanical characterization showed that the interference of the fillers with the UV curing process was the main parameter determining the mechanical performance of the 3D printed materials.

Introduction

Additive manufacturing (AM), also known as 3D printing, is an innovative fabrication technique that has received increased attention over the last few years [1]. Compared to traditional formative methods, it enables faster production of highly individualized items, while generating less waste [2]. Stereolithography is the only AM process that employs thermosetting resins via UV-curing, which allows for the manufacturing of three-dimensional objects with a very high level of details [3]. Epoxide-type polymers and polyester/polyurethane acrylates are the main materials that are employed, and their crosslinking is achieved via cationic and radical polymerization respectively [4,5]. Currently, a wide range of materials is commercially available, however bio-based examples are scarce [6].

To address this issue, research has focused on the development of bio-based systems from renewable monomers [7]. These include formulations based mainly on vegetable oils (VOs) [8,9] and itaconic acid-based unsaturated polyesters [10], while terpene-based monomers have also been investigated [11,12]. VO-based resins have shown excellent printing accuracy comparable to that of expensive, high-resolution commercial resins [13]. However, the resulting mechanical properties are considered inferior to those of commercial resins. Therefore, strategies to enhance the mechanical behavior of these materials have been examined, such as their usage in combination with acrylic monomers [14] or the utilization of nanoinclusions [15]. For example, in the work of Wang et al., nanocellulose was found to be a successful reinforcement agent, showing increased mechanical performance compared to the neat resin [16]. Barkane et al. displayed that the combination of nanocellulose with other lignocellulosic particles like lignin and hemicellulose results in hybrid nanocomposite materials with enhanced thermomechanical performance [17]. Finally, in the work of Jurinovs et al. nanofibrillated cellulose was modified to reduce the agglomeration in the resin and was used to enhance the mechanical performance of the final cured materials at very low filler loadings [18]. From the aforementioned studies, it becomes clear that the preparation of nanocomposites offers the strategic advantage of enhanced mechanical performance without compromising the bio-based content of the materials.

In addition to materials based on (meth)acrylic acid, itaconic acid-based polyester resins have also been identified as potential bio-based binder resins for AM materials, due to the simplicity of their production and the tunability of their thermomechanical profile, which can be equivalent to commercial resins [19–26]. The tuning of the mechanical performance is mainly based on the density of the crosslinking network and on the ability to combine aliphatic and aromatic structures in the polyester backbone [27]. Furthermore, selection of diluent can also assist in the formation of a high mechanical performance network [28]. As a contribution to itaconic acid-based materials for UV-curing additive manufacturing from our labs, we have demonstrated that the thermomechanical performance of these materials can be influenced by the polyester structure, [29] diluent content, [30] and diluent selection. Interestingly, the influence of nanoparticles on the thermomechanical properties of polyester itaconates has not yet been explored. Given the beneficial effect these nanoinclusions have demonstrated in VO-based systems, a similar behavior should be expected for itaconic acid-based systems.

In this work, seven nanocomposite polyesters based on itaconic acid were synthesized, by an *in-situ* polycondensation process to ensure uniform dispersions of the nanoparticles in the polyester resin. Different types of fillers were tested, to determine the effect of filler characteristics on the properties of the final material. Nanocrystalline cellulose was selected as a filler which is expected to interact with the polymer matrix of the cured parts due to the plethora of -OH groups on its surface. Montmorillonite and graphene were selected as inorganic and organic fillers, in the form of nanoplatelets, which are expected to have limited interaction with the polymer matrix. Finally, titanium dioxide was selected as a metal-based filler that has been used in photocatalytic and antimicrobial applications and could therefore broaden the applications for itaconic acid-based materials. The synthesized polyesters were combined with commercial diluents to create formulations suitable for UV-curing additive manufacturing processes. These formulations were subsequently processed on an UV-curing DLP 3Dprinter and their thermomechanical properties were analyzed.

Materials and methods

Materials

Itaconic acid (IA, 99 %) and sebacic acid (SA, 99 %) were purchased from Merck, Darmstadt, Germany. 1,3-Propanediol (1,3- PDO, 99.7 %) was kindly provided by DuPont Tate & Lyle Bio Products, Loudon, NH, USA. 2,6-Di-*tert*-butyl-4-methylphenol (BHT, 99 %) was bought from Merck, Darmstadt, Germany. 4-Methoxyphenol (MeHQ, 99 %) was purchased from Sigma-Aldrich Chemie, Steinheim, Germany. FASCAT® 4101 catalyst was kindly provided by PMC Group, Mount Laurel, NJ, USA. Cellulose nanocrystals, CNC, were purchased from the University of Maine (Orono, Maine, USA) and have dimensions of approximately 5 nm in diameter and 150–200 nm in length. Graphene nanoplatelets, GNPs, were purchased from XG Sciences (under the code name 'xGnP-Grade M') and were of 2.2 g cm^{-3} mass density, 5 μm diameter, 6–8 nm thickness and B120–150 m^2 g^{-1} specific surface area. Montmorillonite, Cloisite®Na+ (MMT), was purchased by Southern Clay products, Gonzales, TX, USA and has an interlayer distance of 11.7 Å. Titanium dioxide (TiO_2) NPs of 3–5 nm in size, were supplied by Cinkarna Celje (CCA 100BS). Acryloyl morpholine (ACMO, 99 %) was purchased from Rahn GmbH,

Table 1

Composition and properties content of the synthesized polyesters.

Sample	IA (eq)	SA (eq)	1,3-PDO (eq)	Filler loading (wt%)	Bio-based content [a] (wt%)	M_n (g/mol)[b]	M_w (g/mol)[b]	Đ	T_g (°C)[c]
PE neat	0.5	0.5	1.45	–	100	980	1980	2.04	< -50 °C
PE-CNC-A				1	100	1060	2590	2.42	
PE-CNC-B				2	100	1110	2220	2	
PE-MMT-A				1	99	1270	2690	2.12	
PE-MMT-B				2	98	1090	2140	1.97	
PE-GNP				0.4	99.6	1120	2480	2.22	
PE-TiO_2-A				1	99	1040	1960	1.89	
PE-TiO_2-B				2	98	1010	1780	1.75	

[a]% of mass of renewable monomers used for the synthesis of each resin, [b] obtained by SEC measurements, [c] estimated by DSC.

Frankfurt, Germany. Diphenyl(2,4,6-trimethylbenzoyl)phosphine oxide (TPO) was purchased from IGM Resins. Chloroform-d_1 (99.8 % D) + 0.03 % TMS v/v was obtained from Carl Roth, Karlsruhe, Germany. Solvents were reagent or analytical grade and were purchased from VWR International, Fontenay-sous-Bois, France.

Polyester synthesis

Eight polyesters were synthesized via azeotropic polycondensation. The diacid to diol ratio used was 1:1.45, in an effort to limit the viscosity of the prepared resins. As an example, the synthesis of resin PE neat is described below. For the synthesis of 100 g of polyester, 42.02 g of SA (0.5 equiv., 0.21 mol), 27.03 g of IA (0.5 equiv., 0.21 mol) and 45.85 g of PDO (1.45 equiv., 0.6 mol), along with 0.06 g of MeHQ (0.06 wt%), 0.08 g of BHT (0.08 wt%) and 0.39 g of FASCAT 4101 (0.39 wt%) were charged into a three necked round bottom flask equipped with an immersed thermocouple to control the temperature of the heating mantle, a mechanical stirrer, and a Dean-Stark condenser. Toluene (10 % w/w) was also added as an azeotropic solvent to facilitate water removal. The mixture was heated gradually until homogenization, and then reacted at 180 °C until an acid value of < 5 mg KOH/g was reached (usually 3-4 h). The toluene was then removed under reduced pressure at 130 °C and 100 mg of MeHQ were added to the resin for stabilization. For the synthesis of the nanocomposite resins, the nanofillers were dispersed into the PDO, by means of sonication with a sonication probe (Sonopuls HD 2070, Bandelin electronic GmbH, Berlin, Germany). After 20 min of sonication, uniform dispersions were created, which were then charged into the reaction flask. The reaction then continued as described for the neat resin. The polyesters were obtained without further purification, as viscous liquids. Polyesters containing nanocellulose were transparent, those containing montmorillonite were yellow, the graphene one was black and the TiO_2 containing polyesters were white. The neat resin was transparent. The description of resin compositions is given in Table 1.

Formulation preparation

To prepare the formulations suitable for additive manufacturing, a mass ratio of polyester: reactive diluent: TPO of 0.5:0.47:0.03 was used. As an example, the preparation of 80 g of Form-neat-A is described. 40.0 g of PE neat, 37.6 g of ACMO and 2.4 g of TPO were introduced to a lid-closing metal can, to prohibit light exposure. The mixture was left under stirring overnight until homogenization and was then used for AM experiments.

Measurements

FTIR spectra of the synthesized resins were obtained on a Thermo Scientific Nicolet iS5 FTIR (Thermo Fisher Scientific, Waltham, MA, USA) using the ATR technique (32 scans, resolution of 4 cm^{-1}).

NMR experiments were conducted on a Magritek Spinsolve 60 MHz Ultra benchtop spectrometer. ^1H NMR shifts of polymers are reported in ppm (δ) downfield from tetramethylsilane (TMS) and were determined by reference to the residual solvent peak (chloroform-d_1, 7.26 ppm for hydrogen atoms).

The acid value (AV) is proportional to the unreacted acid groups. It was defined as the mg of KOH required to neutralize one gram of sample and was determined according to DIN EN ISO 2114 by titrating the carboxylic acid groups of the sample with potassium hydroxide solution in methanol (0.3 mol/L). The sample (1-2 g) taken was dissolved in acetone.

Determination of the molar mass distribution was performed by SEC measurements with tetrahydrofuran as eluent and with polystyrene calibration in the range of 162 g/mol–70,000 g/mol. Three columns SDV 1000A at 40 °C, a variable UV-detector (here: 254 nm), a refractive index detector and the software (WinGPC Unity) were provided by Polymer Standard Service (Mainz, Germany). The samples were filtered over a 0.2 mm PTFE filter prior to injection.

Differential scanning calorimetry (DSC) measurements were conducted on a DSC $^{3+}$ (Mettler-Toledo, Greifensee, Switzerland). For all materials, 10 mg were prepared in 40 µL aluminum crucibles with lids. The measurement starts at -70 °C, then the material is heated up to 140 °C under nitrogen (35 mL min^{-1}) with a heating rate of 10 K min^{-1}. This cooling and heating process are repeated to detect possible changes in material properties. The evaluation was carried out with STARe Software (V.16.20b, Mettler-Toledo, Greifensee, Switzerland).

Viscosity measurements were performed on a Malvern Kinexus lab+ (Malvern Panalytical Ltd, Malvern, UK) equipped with cone-plate geometry (CP 4°, 40 mm). Measurements were made with a rotation speed of 100 s^{-1} for 10 s. Five measurements were made at each temperature, and the average value was calculated.

Photo-differential scanning calorimetry (Photo-DSC) measurements were conducted on a DSC^{3+} (Mettler-Toledo, Greifensee, Switzerland) equipped with a Lightningcure LC8 UV spotlight source (Hamamatsu Photonics, Hamamatsu, Japan) at 70 % of its maximum intensity. This corresponds to an irradiance flux density (light density) of 175 mW/cm^2 provided on the surface of the sample. The lamp used is a mercury-xenon lamp with a broad irradiation spectrum with the highest intensity at 365 nm. To get the integration of the heat of reaction, two runs were carried out with a short break between the runs to let the resin cool down. The second run was made once the material was fully cured, and the baseline was stable. Then, the second curve was subtracted from the first to obtain the curve related to the curing only. Each run is conducted as follows: 30 s at 25 °C at atmospheric pressure under nitrogen without the lamp; then, the lamp is turned on for 4.5 min. The break between the runs lasts 30 s. To calculate the conversion of the C=C double bonds, the assumption was made that acrylate and itaconate double bonds have similar kinetics during homo- and copolymerization, utilizing the theoretical maximum enthalpy liberated by a mole of ACMO (acrylamide was used as reference: $\Delta H_{\text{acrylamide theo}}$: 82.64 kJ/mol) [31,32] and a mole of substituted itaconate (dimethyl itaconate was used as reference: $\Delta H_{\text{DMI theo}}$: 60.67 kJ/mol). [33]

Photo-rheology data were collected by means of Anton Paar 302MC rheometer (Physica MCR 302, Graz, Styria). The rheometer was set with a plate-plate geometry, the outside diameter of the metal disk was 25 mm and a glass disk was used as bottom support in order to guarantee the irradiation of the sample. The distance between the two disks was set at 200 um. The visible-light was provided by optic fiber to directly irradiate the sample. A Hamamatsu LIGHTINGCURE LC8 was used as visible-source with a light intensity of about 40 mW/cm^2 provided on the surface of the sample. The lamp was centered at 405 nm to match the wavelength used during the 3D printing process. For this a A9616-09 UV-filter was used to block the UV-light guaranteeing the emission above 400 nm. The lamp was turned on after 60 s of stabilization and the measurements were performed in oscillatory condition at a frequency of 1 Hz, with strain 1 % and in isothermal condition at room temperature.

Additive manufacturing experiments were conducted on a Phrozen Sonic 4 K DLP printer equipped with a 50 W UV LED array (405 nm). The samples were cured with a layer thickness of 10 μm and an exposure time of 5 s per layer for all formulations. Approximately forty grams of formulation were used to print five rectangle specimens at once, suitable for DMA measurements. After the process, samples were removed from the printer and post-cured in a post-curing light oven (Wanhao Boxman^{-1}) for 30 min. The samples were turned after 15 min to ensure even curing of the specimens.

The morphological features of the nanocomposites were assessed through the Phenom ProX (Netherlands) scanning electron microscope (SEM). The specimens were attached on a metal stub with double-sided carbon tape (Ted Pella, USA) and inserted in the scanning electron microscopy's vacuum chamber using a special charge reduction sample holder. This sample holder is designed to reduce sample charging and eliminate extra sample preparation of non-conductive samples. The voltage was 15 kV and the working distance was 6 mm.

To examine the mechanical response of the print-out components, tensile, compression and bending quasi-static loading experiments were performed to extract the main mechanical properties i.e., elastic and flexural. A universal testing machine Testometric M500-50AT equipped with a 500 N load cell was utilized. At least 5 specimens per experiment were tested to achieve reliable the results. All tests were conducted at room temperature, with a strain rate of 5 mm/min. [34] Tensile and compression tests were performed with uniaxial loading according to international standards ISO527 and ISO604, respectively. "Dog-bone" specimens of 1BA type with a total length of 80 mm, a thickness of 4 mm and a parallel section width of 10 mm were used for the tensile tests and specimens with orthogonal configuration and dimensions of 10 mm x 10 mm x 4 mm were used for compression testing fulfilling the shape and dimensional requirements of the ISO604. Regarding the bending loading tests, the 3-point bending test configuration was chosen and the experiments were conducted according to the ISO178, with orthogonal specimens with dimensions 80 mm x 10 mm x 4 mm.

Nanoindentation was employed in order to identify the micro-hardness of the print-out structures and verify the macroscopic measurements for elastic modulus. For this process, the SHIMADZU DUH-211S Dynamic Ultra Micro Hardness Tester was utilized employed with a Berkovich diamond indenter with a 100 nm tip radius and a force resolution of 0.196 μN. The nanoindentation process was performed, according to the ISO/TS19278, on the 3D printed samples with dimensions of 30 mm x 10 mm x 5 mm. The machine's indenter was regulated to penetrate the sample's surface with an applied force of 20 mN. Furthermore, employing the Oliver–Pharr formula, the elastic modulus and the micro-hardness, in terms of Vickers Pyramid Number (HV), were calculated. [35] More details can be found in Supporting Information and Fig. S1. At least 10 measurements were conducted in scatter regions of each sample to secure the reliability of the results.

Dynamic mechanical analysis (DMA) was carried out on a Tritec 2000 DMA (Triton Technology, Loughborough, UK) in single cantilever bending mode. Measurements were performed on the rectangle bars (25 × 10 × 4 mm) which were prepared with additive manufacturing. Samples were studied under nitrogen in a temperature range of 0–120 °C (2 K min^{-1}, 1 Hz, maximum displacement 0.01 mm). The exact dimensions of specimens were determined before each experiment, and five test bars were measured for each sample.

Thermogravimetric analysis (TGA) of cured resins was performed on a TGA/DSC 1 (Mettler-Toledo, Greifensee, Switzerland) under nitrogen (35 mL min^{-1}). Samples of ca. 10 mg were heated from 25 to 700 °C with a heating rate of 10 K min^{-1}.

Results and discussion

Polymer synthesis

The study presented herein aimed to investigate the effect of nanofillers of different characteristics on the thermomechanical behavior of 3D-printed materials derived from itaconic acid. Based

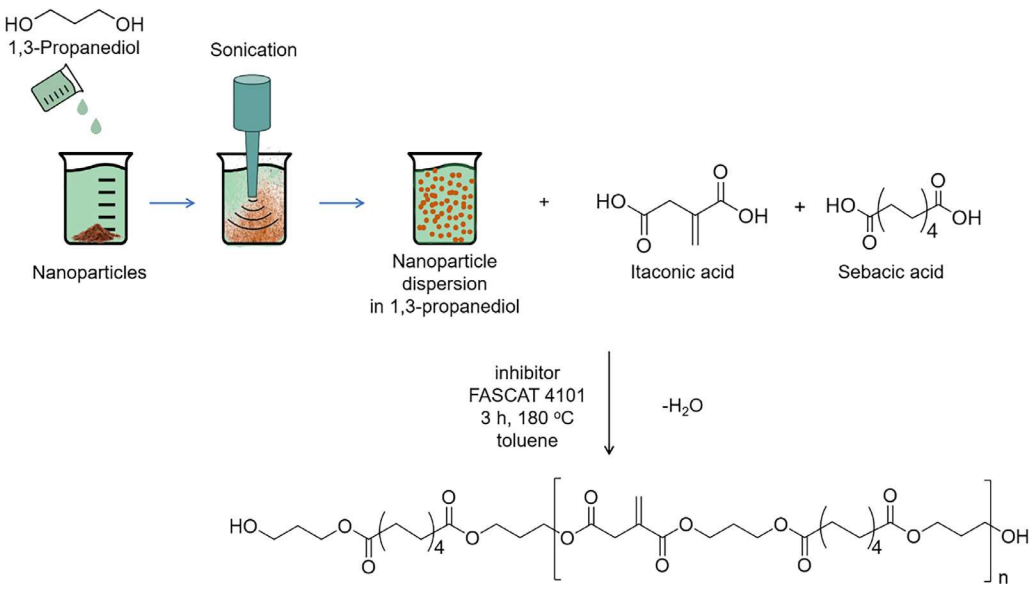

Scheme 1

Synthetic pathway for the polyesters of this study.

on the findings of our previous study, [36] poly(1,3-propylene itaconate-co-sebacate) Scheme 1 with an "average" mechanical performance was selected (regarding its glass transition, the E' Modulus and the elongation at break), to allow for a clear assessment of the effect of the nanofillers on the thermal and mechanical properties. Except for GNPs, two nanocomposite resins were synthesized for each filler type, at 1 and 2 wt% content. For the GNPs containing polyester, preliminary results showed that 0.4 wt% was the maximum content that could be used while maintaining the same AM parameters as the rest of the materials, as the black nature of the GNP absorbed the UV-light. The pristine polyester along with the CNC nanocomposites were transparent. In the case of MMT nanocomposites, the polyesters were opaque and yellow. The GNP and TiO_2 containing resins were black and white, respectively. All resins were stored in the lab, protected from sunlight at ambient temperature. The dispersion of the nanofillers was stable for a period of at least six months, as no sedimentation was observed during that time.

Structural characterization

ATR and ^1H NMR spectroscopy

The ATR spectra of the prepared resins are shown in Fig. S2. For all polyesters, the main vibrations for this class of polyesters are clearly visible. The C=O stretching of the ester bond is found at 1730 cm^{-1}, while the =C-H bending and C=C stretch vibrations of itaconic acid are located at 810 cm^{-1} and 1640 cm^{-1}, respectively. The -OH end groups are visible as a broad signal at 3500 cm^{-1}. Regarding the nanofillers, there are no distinctive signals in the spectra of the nanocomposite resins, as a result of the relatively low concentration and also of the overlapping of the signals derived from the fillers with those of the pristine polyester. Similar results were obtained from the ^1H NMR spectra, which are presented in Fig. S3. The methylene group of the backbone of itaconic acid can be found at 3.3 ppm. The protons of the double bond of itaconic acid are located at 5.7 and 6.3 ppm, respectively. No signals that would suggest isomerization of itaconic to mesaconic acid were detected [37]. For the protons of 1,3-propanediol, the middle methyl group is found at 2.0 ppm, while the free -OH groups are found at 3.7 ppm. The protons of the ester bond are observed between 4.0 and 4.3 ppm. Finally, the methylene groups of SA corresponding to the –OC(O)CH_2– group are located around 2.3 ppm, accompanied by two signals at 1.3 and 1.6 ppm attributed to the internal methylene groups of SA. There are no signals associated with the nanofillers in all collected spectra, due to their low concentration in the polyesters. In all, the collected spectra confirm the successful synthesis of the discussed polyesters.

Physicochemical characterization

In Fig. 1, SEC elugrams are presented. The gaussian distribution is observed for all synthesized materials, a typical feature for polycondensation products. Corroborating ATR and NMR data, the lack of any high molecular weight fractions on the elugrams proves that no partial cross-linking or Ordelt-reaction occurred during the synthesis of the resins. The M_n of the polyesters are in the range of 1000–1300 g/mol and the dispersity Đ is close to 2, regardless of the filler. Finally, DSC measurements were conducted to determine the glass transition. Results are given in Fig. S4. Their T_g is expected below -50 °C, as a result of their aliphatic character and the low molecular weight. Both SEC and DSC results are summarized in Table 1.

Formulation characterization

Polymers designed for UV-curing AM are usually combined with reactive diluents, to enhance printability-related properties like viscosity or reactivity towards UV light. The use of reactive diluents can also be beneficial to the thermomechanical properties of the fabricated specimens, as it allows for higher conversion of

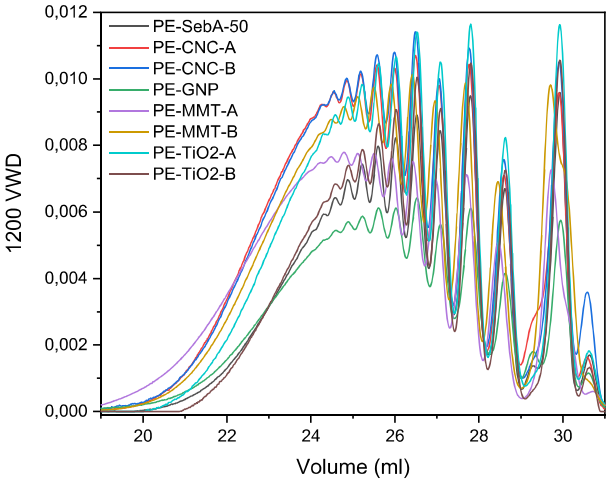

Fig. 1

SEC elugrams of the synthesized polyesters.

the available double bonds. In this work, we selected ACMO as a reactive diluent, as in our previous studies it has shown great compatibility with itaconic acid-based systems [29]. Formulations containing 47 wt% of reactive diluent were prepared for all the nanocomposite polyesters, and their behavior was studied, with regard to viscosity and reactivity towards UV-light. The composition of the formulations, their bio-based content, their viscosity and the results of the photo-DSC are summarized in Table 2.

Photo DSC

The reactivity of the formulations towards UV-irradiation was examined by means of photo DSC and the results are presented in Fig. 2. From the preparation phase, it was clear that the optical properties of the formulations were dictated by the fillers' addition. Formulations containing MMT, GNP and TiO_2 retained the color of the respective filler (light yellow, black and white respectively). CNC-containing formulations were an exception, as they were transparent like the formulation of the pristine resin. As a result, the reactivity of the formulations was greatly influenced. While the polymerization rate of the CNC-containing formulations was equivalent to that of the pristine formulations, it was significantly reduced for the rest of the formulations. Furthermore, regardless of the filler type, the addition of higher amounts of filler resulted in lower reactivity towards UV-induced crosslinking. The addition of GNPs led to the highest reduction of the polymerization rate, followed by TiO_2 and MMT (Form-GNP had a higher ROP_{max} compared to Form-TiO_2, but only it contained only 0.2 wt% of filler compared to 0.5 and 1 wt% for the TiO_2 containing formulations). This behavior also affected the overall C=C conversion. In the case of the transparent resins, the slight lowering of the ROP in the nanocomposites resulted in a higher conversion of the double bonds, in a manner similar to our previous study [30]. However, the rest of the formulations exhibited reduced conversion, probably due to scattering and absorption phenomena caused by the addition of the filler. As observed for the ROP_{max}, the addition of higher filler amounts into the formulation lowered the overall conversion.

Photorheology

To corroborate the results of photo DSC analysis, photorheology tests were performed. Results are given in Fig. 3, which shows the evolution of storage modulus and normal force over time. Light irradiation was turned on after 60 s of stabilization and all nanocomposite formulations presented a delay compared to the pristine one. This delay is associated with the coloration of the nanocomposite formulations, as the increment of the induction time was proportional to their reduced transparency. Moreover, the amount of filler in the formulations also affected their reactivity, as the increment from 0.5 to 1 wt% resulted in higher time delay suggesting that the filler addition was responsible for the reduced reactivity towards UV-light, similar to the photo DSC results. GNP was found to be the least beneficial filler regarding the reactivity of the formulation, as Form-GNP presented the highest delay of all samples, even though it had the lowest filler concentration (0.2 wt%). This can be attributed to the high absorption and blocking effect of the filler. Nevertheless, regardless of the filler type, the slope of the storage modulus' increase was similar for all formulations, suggesting that the inclusions did not inhibit, but just delayed the polymerization of the system.

Another parameter that was monitored by photorheology measurements and provides useful information about the formulations is the evolution of "normal force" over time. The term describes the force required to maintain the distance between

Table 2

Viscosity and UV-DSC results of the prepared formulations.

Formulation	Resin (50 wt%)	Reactive Diluent (47 wt%)	Nanoparticle (wt%)	Bio-based content (wt%)[a]	Viscosity @ 20 °C (Pa*s)	RoP ($s^{-1}*10^3$)	C %
Form neat	PE neat	ACMO	–	50	0.15	83.2	89.3
Form-CNC-A	PE-CNC-A		0.5	50	0.20	79	93.4
Form-CNC-B	PE-CNC-B		1	50	0.20	76.5	88.8
Form-GNP	PE-GNP		0.2	49.8	0.21	59.8	81.7
Form-MMT-A	PE-MMT-A		0.5	49.5	0.26	73.7	82.8
Form-MMT-B	PE-MMT-B		1	49	0.25	68.4	78.7
Form-TiO_2-A	PE-TiO_2-A		0.5	49.5	0.23	51	80.7
Form-TiO_2-B	PE-TiO_2-B		1	49	0.25	45.5	80.1

[a]% of mass of renewable components in the formulation

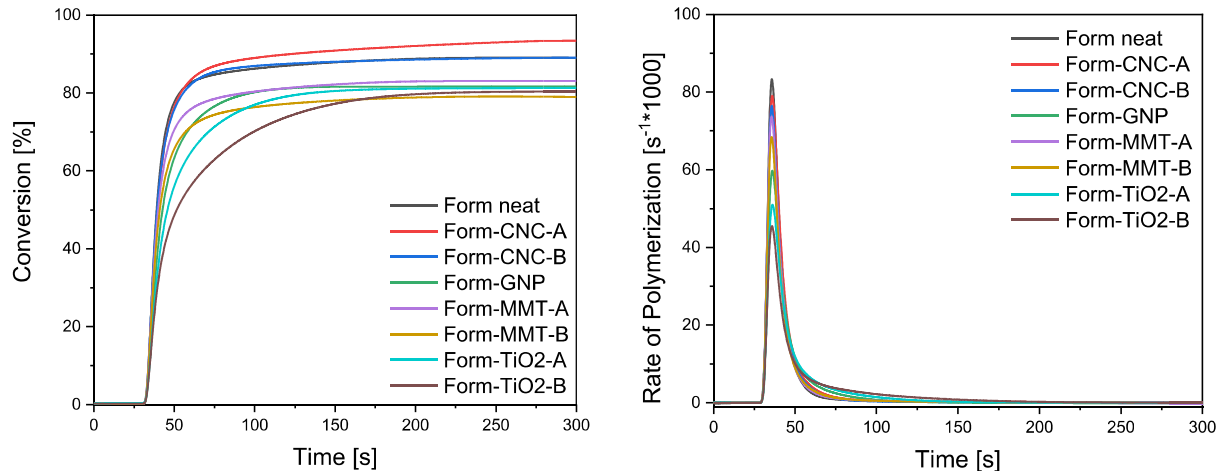

Fig. 2

Photo-DSC results of the prepared formulations: Conversion (left), rate of polymerization (right).

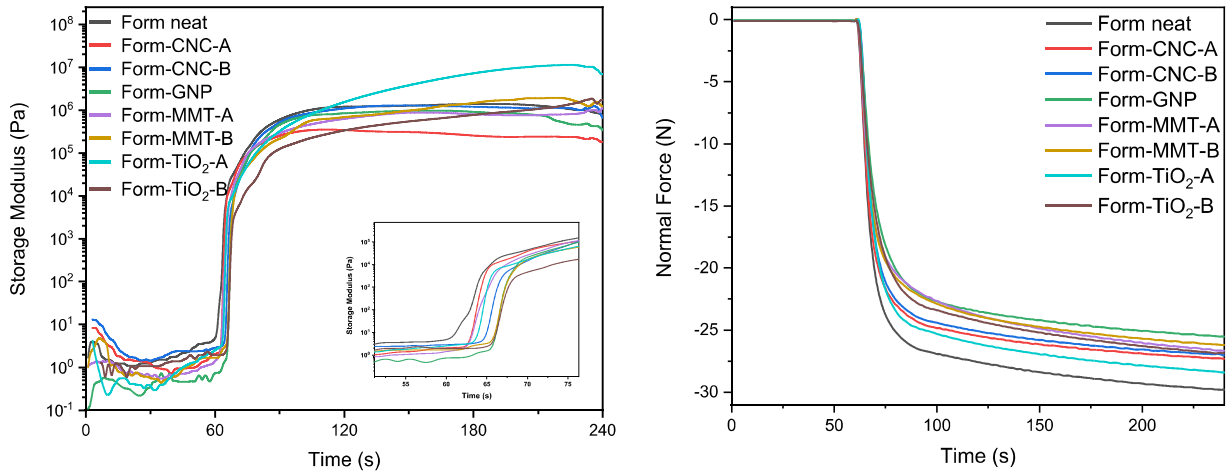

Fig. 3

Photo rheology measurements of the prepared formulations: Evolution of the Storage Modulus (G') (left) and the Normal Force (right) over time.

the glass substrate and the rotating disk constant, and it has been connected to shrinkage induced by radical crosslinking [38]. All nanocomposite formulations recorded lower (absolute) normal force values compared to the neat formulation, suggesting a reduction in shrinkage. This result is associated with the fact that the nanoparticles are not part of the crosslinking network, and they retain their original volume through the polymerization process. Finally, GNPs were the most beneficial inclusion regarding dimensional stability, as Form-GNP presented the lowest normal force value while also containing the lowest amount of filler.

Printed samples

Having examined the reactivity of our formulations in depth, test specimen were manufactured by a DLP 3D printing process. Given that the nanofillers were found to interfere with the UV light pathway (hindering, absorbing etc.), a layer thickness of 10 μm was selected to minimize the effect of the filler and successfully manufacture specimens for evaluation of the mechanical properties. Printed specimens are presented in Fig. 4. Beside specimens for mechanical characterizations, the formulations were utilized to fabricate more complex structures, replicating intricate computer aided designs (CADs) as dentistry geometries require. An example is reported in Fig. 6, showing the feasibility to replicate such geometries with detail and accuracy.

In the preparation of nanocomposite materials, filler dispersion is a very important parameter, as it often influences their mechanical performance. To evaluate it, the 3D printed specimens were analyzed by EDS. EDS was used to monitor the silicon and aluminum atoms of montmorillonite, and the titanium atoms of TiO_2, on the fracture surface of the specimens used for the tensile measurements. In the case of cellulose and graphene, no such observation could be made, as both the fillers and the polymer matrix are constituted of carbon and oxygen atoms, therefore they could not be differentiated. Results are presented in Figs. 5 and S5.

Comparing the two nanocomposite materials containing TiO_2 nanoparticles, it was clear that the material with the lowest filler content presented a more homogenous distribution (Fig. 5

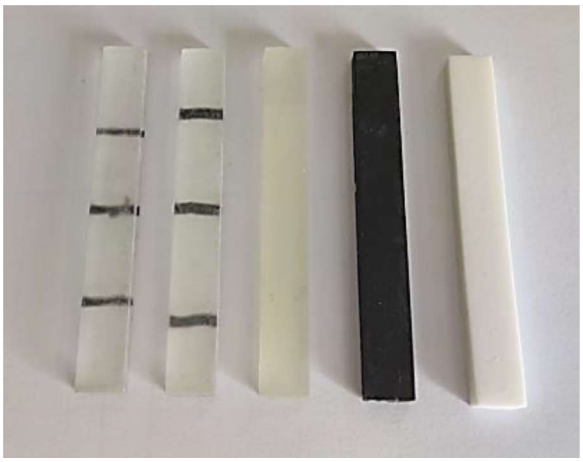

Fig. 4

Printed specimens for mechanical characterizations. From left to right: 3D-neat, 3D-CNC-A, 3D-MMT-A, 3D-GNP, 3D-TiO_2-A.

top). Though titania particles could be observed throughout the polymer matrix, small aggregations were observed in 3D-TiO_2-A and slightly bigger ones for 3D-TiO_2-B. This result suggests that while *in-situ* polymerization can achieve dispersion of the fillers through the matrix, it cannot completely eliminate the aggregation of the fillers. A similar result was obtained for the MMT containing nanocomposites (Fig. S5), as in the case of 3D-MMT-B, clusters could be observed in different regions of the sample. Those clusters could potentially contribute to the lower C=C conversion that was recorded every time the filler content was increased, as they could block the UV-light more effectively. Furthermore, agglomeration of nanofillers is often associated with inferior mechanical behavior, as in such spots phase separation between the polymer matrix and the filler is observed and they are prone to mechanical failure under stress.

Thermomechanical characterization

Fig. 7 illustrates the experimental curves extracted for tensile and compression tests. The values of the main mechanical properties of the developed composite materials are listed in Table 3. Through the tensile and compression testing, the elastic properties of the examined materials were evaluated, namely elastic modulus, yield stress, and ultimate tensile strength (UTS), along with the corresponding stress-strain diagrams. From these results, it was observed that the PE-CNC resins revealed the highest stiffness and strength compared with all other examined materials, with PE-CNC-A having a slightly better overall performance than PE-CNC-B (micro-hardness of 5.87 and 4.95 HV, respectively). On the other hand, the lowest stiffness and strength were observed for the PE-TiO_2 resins with limited plasticity (elongation at break <20 %), probably due to the lower

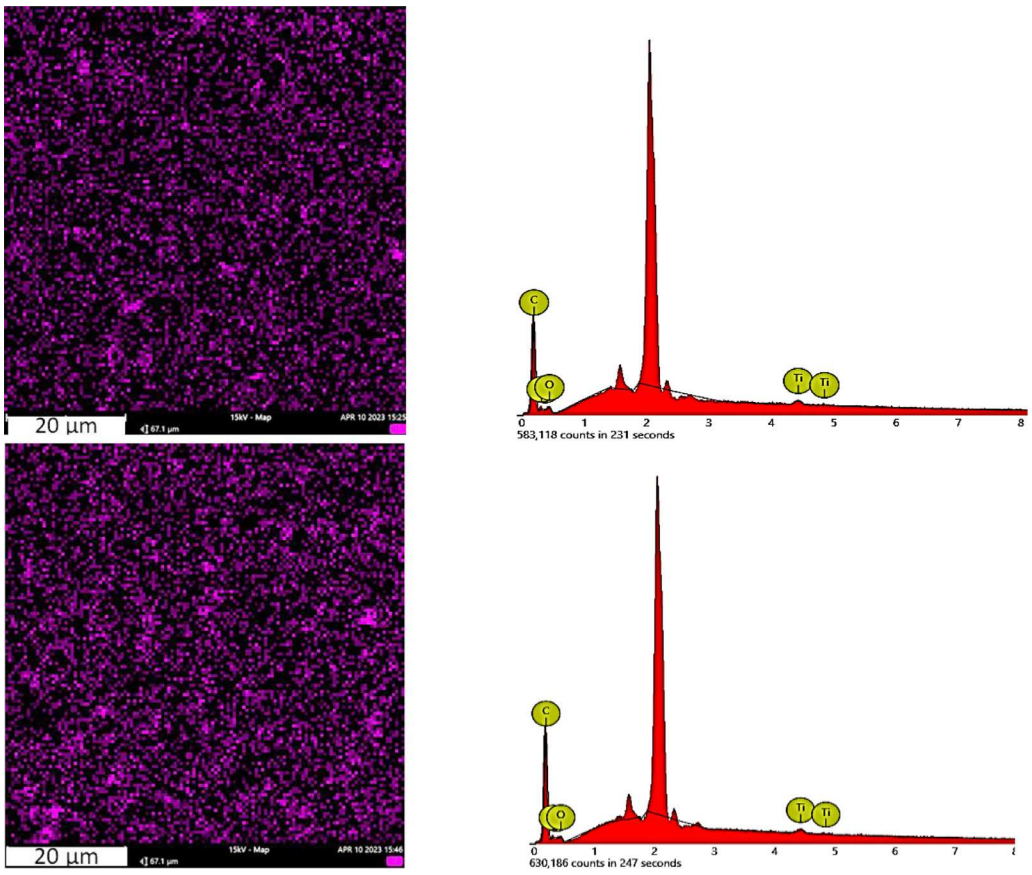

Fig. 5

EDS mapping of 3D-TiO_2-A (top) and 3D-TiO_2-B (bottom).

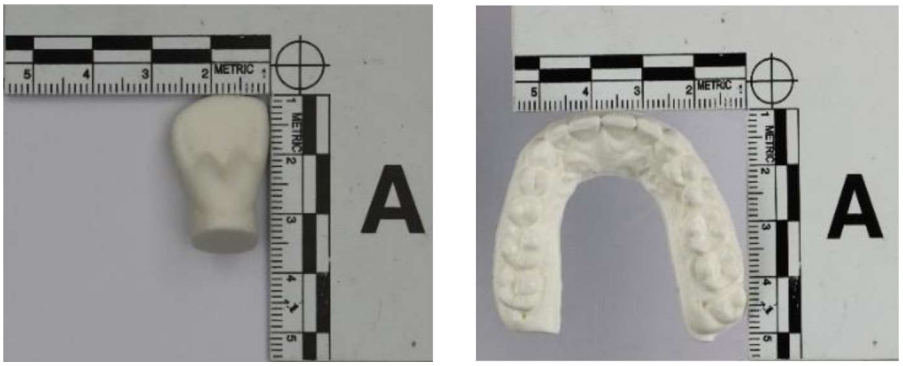

Fig. 6

Denture replicas printed from 3D-TiO_2-A.

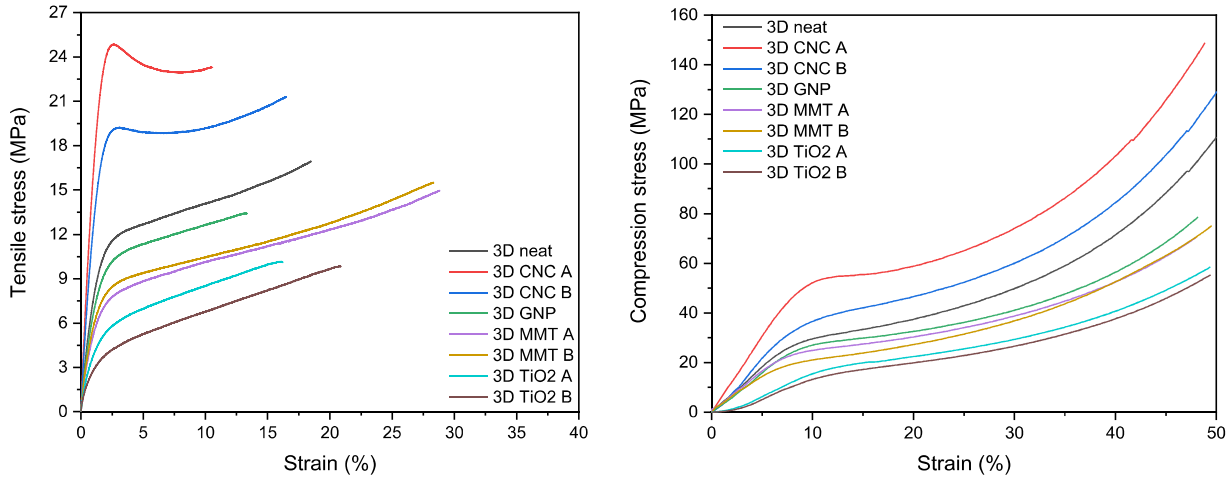

Fig. 7

Tensile (left) and compression (right) stress vs strain of the nanocomposite specimens.

Table 3

Summary of the mechanical properties of the fabricated nanocomposite materials.

Sample	Elastic Modulus (MPa)	Yield Stress (MPa)	Ultimate Tensile Strength (MPa)	Elongation at break (%)	Max. Deflection Force (N)	Flexural Modulus (MPa)	Flexural Strength (MPa)
3D neat	600 ± 50	8.8 ± 1	16.9 ± 1.5	18.3 ± 2.5	73.4 ± 5	467 ± 50	33.5 ± 2
3D-CNC-A	1520 ± 85	20.3 ± 1.5	24.5 ± 1.5	10.2 ± 2	98.6 ± 7	623 ± 70	46.2 ± 3
3D-CNC-B	1350 ± 80	17.5 ± 1.5	21.3 ± 1.5	16.5 ± 1.5	86.7 ± 7	535 ± 50	40.6 ± 3
3D-GNP	860 ± 50	9.4 ± 1	13.4 ± 1.5	13.4 ± 1.5	52.9 ± 3	326 ± 30	24.8 ± 2
3D-MMT-A	514 ± 50	7.2 ± 1	15 ± 1.5	28.8 ± 3	28.6 ± 2	187 ± 15	13.4 ± 1
3D-MMT-B	590 ± 50	7.8 ± 1	15.5 ± 1.5	28.4 ± 1.5	40.6 ± 3	229 ± 15	17.4 ± 1
3D-TiO_2-A	450 ± 50	4.5 ± 0.5	10.2 ± 1	16.5 ± 2	10.1 ± 0.5	63 ± 10	4.8 ± 0.5
3D-TiO_2-B	300 ± 50	3.2 ± 0.5	9.9 ± 1	20.1 ± 2.5	10.6 ± 0.5	66 ± 10	5 ±0.5

conversion of the C=C double bonds compared with the materials containing the CNC nanoparticles.

Furthermore, MMT had a positive effect on the elongation compared to the neat resin, reaching an elongation of 28 % with UTS 15 MPa, compared to 18 % and 17 MPa for the neat resin. Neat PE showed a soft polymer behavior, and the insertion of CNC improved its mechanical behavior, reaching similar stiffness behavior which is usually observed with thermoplastic 3D-printed polyamide 12 (PA12) [39]. This can potentially be explained by the increased interactions between the polymer matrix and this nanofiller, due to the plethora of -OH groups, as previously reported for epoxy-based systems [9]. The mechanical performances of the materials are visible in the stress-strain diagrams (Fig. 7), where typical curves for thermoset materials were obtained for the majority of the materials, with the exception of the PE-CNC resins where a softening effect could be observed. Regarding the flexural properties, similar behaviors were observed with the elastic properties for all examined composite materials.

Table 4

Summary of nanoindentation, DMA and TGA results.

Sample	Microhardness (HV)	tan δ (°C)	E′ @25 °C (MPa)	$T_{5\,\%}$ (°C)	T_{max} (°C)
3D neat	2.43 ± 0.3	69	250 ± 40	320	403
3D-CNC-A	5.87 ± 0.5	73	260 ± 20	329.3	402
3D-CNC-B	4.95 ± 0.5	67	240 ± 20	326.7	403.2
3D-GNP	2.42 ± 0.3	61	200 ± 10	317.3	402.7
3D-MMT-A	2.27 ± 0.3	58	185 ± 5	322.7	403
3D-MMT-B	2.32 ± 0.3	53	150 ± 10	312.3	408.2
3D-TiO_2-A	2.32 ± 0.1	67	210 ± 30	287.5	403.2
3D-TiO_2-B	2.28 ± 0.1	68	260 ± 30	268	402.5

Finally, through the nanoindentation tests, the values of elastic modulus were verified and the micro-hardness of each developed resin was evaluated. Regarding the micro-hardness of the examined materials, the extracted results were consistent with nanocomposite thermosets according to the Granta CES material library (EDU pack 2012), both in graphical form and in the micro-hardness values, as it is presented in Fig. S6 and Table 4, respectively. Moreover, the differences in the micro-hardness values were negligible with the only exception, the PE-CNC materials which revealed sufficiently higher micro-hardness, supporting the results obtained from the tensile measurements. Nevertheless, it must be noted that the obtained value was lower in the case of the material with the higher CNC concentration, suggesting that there is a balance point to be reached, between the reinforcing effect of the fillers and the lowering of the C=C conversion, to extract the maximum mechanical performance out of these materials.

DMA

The thermomechanical behavior of the fabricated specimens was also assessed *via* DMA measurements and the results are presented in Fig. 8. The glass transition temperature of the samples was in the range of 53–73 °C. Materials containing montmorillonite recorded the lowest values, in accordance with the photo DSC measurements where the lowest C=C conversion was recorded. As it was observed in previous studies, [30] the double bond density and the conversion are the primary parameters that influence the mechanical behavior of the 3D printed materials. The absorption of UV-light by the fillers during the manufacturing stage inhibits the polymerization and therefore limits the mechanical performance of the materials. This is supported by the fact that the materials containing nanocellulose demonstrated the highest values of elastic modulus and glass transition temperature, similar or slightly better compared to the pristine material. Those materials were also found to be the most reactive ones among the nanofiller-containing formulations in the photo DSC experiments. GNP-containing material recorded slightly higher T_g and E′ Modulus values compared to the MMT-containing materials but given that its filler content was five times lower it is probable that with equal filler content, its mechanical properties would be inferior to the MMT materials. Finally, the TiO_2 materials, despite the lower C=C conversion record similar mechanical properties with the pristine and the CNC-containing materials. The results are summarized in Table 4.

TGA

The thermal stability of the samples was also investigated by means of TGA measurements. The results are presented in Fig. 9

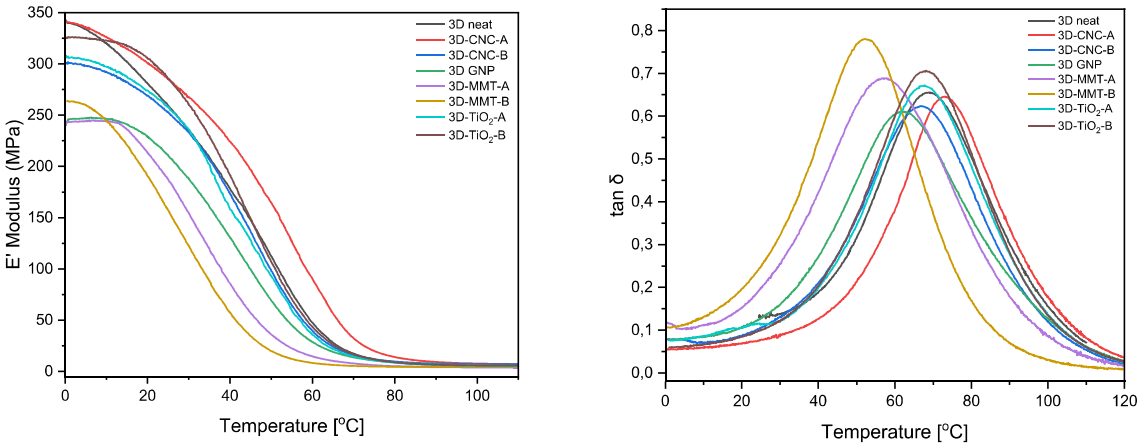

Fig. 8

DMA results of the 3D printed materials.

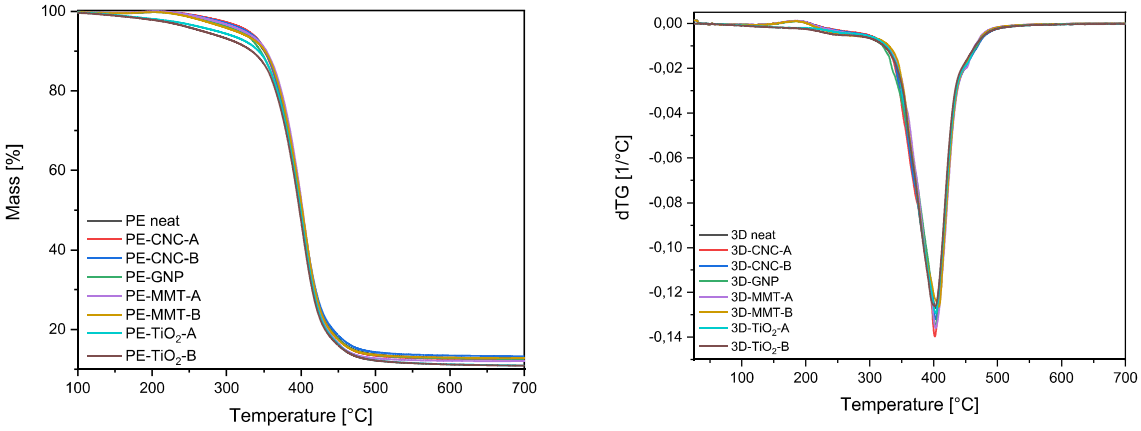

Fig. 9

TGA results of the nanocomposite materials.

and the main values are summarized in Table 4. Following the trend that was already set from the assessment of reactivity towards UV-light, materials containing high concentrations of the filler (materials type B, 1 wt%) displayed lower thermal stability than the materials with low concentrations of the filler (type A, 0.5 %). This behavior is connected to the higher C=C conversions that were recorded for the materials of low filler concentration. In fact, the C=C conversions were found to be the key parameter that influenced the thermal stability of the nanocomposite materials. Indeed, nanocomposites containing CNC that were transparent and highly reactive had improved $T_{d,5\ \%}$ compared to the pristine material. On the other hand, the materials containing TiO_2 were found to be the least thermally stable, as the TiO_2 particles hindered light penetration. Nevertheless, all materials exhibited $T_{d,5\ \%}$ above 250 °C, which is adequate for common applications.

Conclusions

The study presented herein focused on examining the impact of nanofillers on the properties of 3D printed materials derived from itaconic acid. This investigation was approached through the *in-situ* synthesis of a series of nanocomposite polyesters, incorporating fillers with varying geometries and chemistries. While the physicochemical properties of the polyesters remained unaffected by the inclusions, the reactivity of the formulations underwent significant changes based on the filler type, concentration, and the formulations' transparency. Notably, nanocellulose emerged as the most effective reinforcing agent as a result of the increased interactions due to the free -OH groups, while graphene substantially reduced formulation reactivity, limiting its application to very low concentrations. The dispersion of the fillers in the matrix was adequate but could be improved, potentially by surface modification of the fillers, in order to achieve more homogenous materials. Finally, the evaluation of the thermomechanical properties of the 3D-printed materials revealed that reactivity towards UV-light and C=C conversion were the primary factors influencing their mechanical performance. The bio-based nanocomposites were successfully 3D printed by DLP, achieving good result in terms of accuracy demonstrating the feasibility as greener substitutes to fossil-based resins for several applications.

This publication is based upon work from COST ActionFUR4Sustain, CA18220, supported by COST (European Cooperation in Science and Technology). The authors would like to thank Anja Gohla, Kirsten Wittenberg and Emmanouil Tzimtzimis for their help with TGA, viscosity and SEM/EDS measurements.

Declaration of competing interest

The authors declare the following financial interests/personal relationships which may be considered as potential competing interests: Lazaros Papadopoulos reports travel was provided by European Cooperation in Science and Technology.

Data availability

The data that support the findings of this study are available from the corresponding author upon reasonable request.

CRediT authorship contribution statement

Lazaros Papadopoulos: Writing – original draft, Visualization, Investigation, Conceptualization. **Lorenzo Pezzana:** Writing – review & editing, Visualization, Investigation. **Natalia Malitowski:** Visualization, Investigation. **Nikolaos Kladovasilakis:** Writing – review & editing, Investigation. **Dimitrios Tzetzis:** Writing – review & editing, Investigation. **Marco Sangermano:** Writing – review & editing, Supervision, Resources. **Dimitrios N. Bikiaris:** Writing – review & editing, Supervision, Resources, Formal analysis, Conceptualization. **Tobias Robert:** Writing – review & editing, Validation, Supervision, Resources, Project administration, Methodology, Formal analysis, Conceptualization.

Acknowledgments

The research work was supported by the Hellenic Foundation for Research and Innovation (HFRI) under the 3rd Call for HFRI PhD Fellowships (Fellowship Number:6186).

Supplementary materials

Supplementary material associated with this article can be found, in the online version, at doi:10.1016/j.giant.2024.100275.

References

[1] S.C. Ligon, R. Liska, J. Stampfl, M. Gurr, R. Mülhaupt, Polymers for 3D printing and customized additive manufacturing, Chem. Rev. 117 (2017) 10212–10290, doi:10.1021/acs.chemrev.7b00074.

[2] U.M. Dilberoglu, B. Gharehpapagh, U. Yaman, M. Dolen, The role of additive manufacturing in the era of industry 4.0, Procedia Manuf. 11 (2017) 545–554, doi:10.1016/j.promfg.2017.07.148.

[3] E.M. Maines, M.K. Porwal, C.J. Ellison, T.M. Reineke, Sustainable advances in SLA/DLP 3D printing materials and processes, Green Chem. 23 (2021) 6863–6897, doi:10.1039/D1GC01489G.

[4] M. Shahbazi, H. Jäger, Current status in the utilization of biobased polymers for 3D printing process: a systematic review of the materials, processes, and challenges, ACS Appl. Bio Mater. 4 (2021) 325–369, doi:10.1021/acsabm.0c01379.

[5] L. Pezzana, R. Wolff, G. Melilli, N. Guigo, N. Sbirrazzuoli, J. Stampfl, R. Liska, M. Sangermano, Hot-lithography 3D printing of biobased epoxy resins, Polymer (2022) 254 (Guildf), doi:10.1016/j.polymer.2022.125097.

[6] V.S.D. Voet, J. Guit, K. Loos, Sustainable photopolymers in 3D printing: a review on biobased, biodegradable, and recyclable alternatives, Macromol. Rapid. Commun. 42 (2021), doi:10.1002/marc.202000475.

[7] G. John, S. Nagarajan, P.K. Vemula, J.R. Silverman, C.K.S. Pillai, Natural monomers: a mine for functional and sustainable materials – Occurrence, chemical modification and polymerization, Prog. Polym. Sci. 92 (2019) 158–209, doi:10.1016/j.progpolymsci.2019.02.008.

[8] M. Lebedevaite, J. Ostrauskaite, E. Skliutas, M. Malinauskas, Photoinitiator free resins composed of plant-derived monomers for the optical μ-3D printing of thermosets, Polymers (2019) 11 (Basel), doi:10.3390/polym11010116.

[9] L. Pezzana, R. Wolff, J. Stampfl, R. Liska, M. Sangermano, High temperature vat photopolymerization 3D printing of fully bio-based composites: green vegetable oil epoxy matrix & bio-derived filler powder, Addit. Manuf. 79 (2024) 103929, doi:10.1016/j.addma.2023.103929.

[10] S. Pérocheau Arnaud, N.M. Malitowski, K. Meza Casamayor, T. Robert, Itaconic acid-based reactive diluents for renewable and acrylate-free UV-curing additive manufacturing materials, ACS Sustain. Chem. Eng. 9 (2021) 17142–17151, doi:10.1021/acssuschemeng.1c06713.

[11] A.C. Weems, K.R. Delle Chiaie, R. Yee, A.P. Dove, Selective reactivity of myrcene for vat photopolymerization 3D printing and postfabrication surface modification, Biomacromolecules 21 (2020) 163–170, doi:10.1021/acs.biomac.9b01125.

[12] E. Constant, O. King, A.C. Weems, Bioderived 4D printable terpene photopolymers from limonene and β-myrcene, Biomacromolecules 23 (2022) 2342–2352, doi:10.1021/acs.biomac.2c00085.

[13] C. Vazquez-Martel, L. Becker, W.V. Liebig, P. Elsner, E. Blasco, Vegetable oils as sustainable inks for additive manufacturing: a comparative study, ACS Sustain. Chem. Eng. 9 (2021) 16840–16848, doi:10.1021/acssuschemeng.1c06784.

[14] M. Lebedevaite, J. Ostrauskaite, E. Skliutas, M. Malinauskas, Photocross-linked polymers based on plant-derived monomers for potential application in optical 3D printing, J. Appl. Polym. Sci. 137 (2020), doi:10.1002/app.48708.

[15] N. Vidakis, M. Petousis, N. Michailidis, J.D. Kechagias, N. Mountakis, A. Argyros, O. Boura, S. Grammatikos, High-performance medical-grade resin radically reinforced with cellulose nanofibers for 3D printing, J. Mech. Behav. Biomed. Mater. 134 (2022), doi:10.1016/j.jmbbm.2022.105408.

[16] B. Wang, J. Zhou, Z. Wang, S. Mu, R. Wu, Z. Wang, Cellulose nanocrystal/plant oil polymer composites with hydrophobicity, humidity-sensitivity, and high wet strength, Carbohydr. Polym. 231 (2020), doi:10.1016/j.carbpol.2019.115739.

[17] A. Barkane, E. Kampe, S. Gaidukovs, New reinforcing approach for biobased UV-curing resins: hybrid lignocellulose fillers with improved synergy and wood structure mimics, ACS Sustain. Chem. Eng. (2022), doi:10.1021/acssuschemeng.2c07288.

[18] M. Jurinovs, A. Barkane, O. Platnieks, S. Beluns, L. Grase, R. Dieden, M. Staropoli, D.F. Schmidt, S. Gaidukovs, Vat photopolymerization of nanocellulose-reinforced vegetable oil-based resins: synergy in morphology and functionalization, ACS Appl. Polym. Mater. (2023), doi:10.1021/acsapm.3c00245.

[19] V. Vetri Buratti, A. Sanz De Leon, M. Maturi, L. Sambri, S.I. Molina, M. Comes Franchini, Itaconic-acid-based sustainable poly(ester amide) resin for stereolithography, Macromolecules 55 (2022) 3087–3095, doi:10.1021/acs.macromol.1c02525.

[20] M. Maturi, C. Pulignani, E. Locatelli, V. Vetri Buratti, S. Tortorella, L. Sambri, M. Comes Franchini, Phosphorescent bio-based resin for digital light processing (DLP) 3D-printing, Green Chem. 22 (2020) 6212–6224, doi:10.1039/D0GC01983F.

[21] B.Z. Fidanovski, P.M. Spasojevic, V.V. Panic, S.I. Seslija, J.P. Spasojevic, I.G. Popovic, Synthesis and characterization of fully bio-based unsaturated polyester resins, J. Mater. Sci. 53 (2018) 4635–4644, doi:10.1007/s10853-017-1822-y.

[22] V.V. Panic, S.I. Seslija, I.G. Popovic, V.D. Spasojevic, A.R. Popovic, V.B. Nikolic, P.M. Spasojevic, Simple one-pot synthesis of fully biobased unsaturated polyester resins based on itaconic acid, Biomacromolecules 18 (2017) 3881–3891, doi:10.1021/acs.biomac.7b00840.

[23] S. Brännström, M. Finnveden, M. Johansson, M. Martinelle, E. Malmström, Itaconate based polyesters: selectivity and performance of esterification catalysts, Eur. Polym. J. 103 (2018) 370–377, doi:10.1016/j.eurpolymj.2018.04.017.

[24] S. Brännström, E. Malmström, M. Johansson, Biobased UV-curable coatings based on itaconic acid, J. Coat. Technol. Res. 14 (2017) 851–861, doi:10.1007/s11998-017-9949-y.

[25] J. Dai, S. Ma, Y. Wu, L. Han, L. Zhang, J. Zhu, X. Liu, Polyesters derived from itaconic acid for the properties and bio-based content enhancement of soybean oil-based thermosets, Green Chem. 17 (2015) 2383–2392, doi:10.1039/C4GC02057J.

[26] J. Dai, S. Ma, N. Teng, X. Dai, X. Shen, S. Wang, X. Liu, J. Zhu, 2,5-furandicarboxylic acid- and itaconic acid-derived fully biobased unsaturated polyesters and their cross-linked networks, Ind. Eng. Chem. Res. 56 (2017) 2650–2657, doi:10.1021/acs.iecr.7b00049.

[27] S. Ma, T. Li, X. Liu, J. Zhu, Research progress on bio-based thermosetting resins, Polym. Int. 65 (2016) 164–173, doi:10.1002/pi.5027.

[28] Q. Li, S. Ma, X. Xu, J. Zhu, Bio-based unsaturated polyesters, in: Unsaturated Polyester Resins, Elsevier, 2019, pp. 515–555, doi:10.1016/B978-0-12-816129-6.00020-X.

[29] L. Papadopoulos, N.M. Malitowski, D. Bikiaris, T. Robert, Bio-based additive manufacturing materials: an in-depth structure-property relationship study of UV-curing polyesters from itaconic acid, Eur. Polym. J. 186 (2023) 111872, doi:10.1016/j.eurpolymj.2023.111872.

[30] L. Papadopoulos, L. Pezzana, N.M. Malitowski, M. Sangermano, D.N. Bikiaris, T. Robert, UV-curing additive manufacturing of bio-based thermosets: effect of diluent concentration on printing and material properties of itaconic acid-based materials, ACS Omega 8 (2023) 31009–31020, doi:10.1021/acsomega.3c02808.

[31] S. Ohshima, K. Chiba, Y. Ariyama, Z. Ogawa, Kawamura, inventors; Nitto Chemical Industries, assignee, Polymerization of acrylamide in the presence of water-soluble compounds, 1976 US Patent 3,951,934A.

[32] N. Xiang, C. Li, K. Yang, C. Yang, H. Guo, C. Wang, Energy saving technology of acrylamide polymerization in plate reactor based on phase change heat transfer, Appl. Therm. Eng. 227 (2023) 120358, doi:10.1016/j.applthermaleng.2023.120358.

[33] F.S. Dainton, K.J. Ivin, D.A.G. Walmsley, The heats of polymerization of some cyclic and ethylenic compounds, Trans. Faraday Soc. 56 (1960) 1784, doi:10.1039/tf9605601784.

[34] C.R. Siviour, J.L. Jordan, High strain rate mechanics of polymers: a Review, J. Dyn. Behav. Mater. 2 (2016) 15–32, doi:10.1007/s40870-016-0052-8.

[35] W.C. Oliver, G.M. Pharr, An improved technique for determining hardness and elastic modulus using load and displacement sensing indentation experiments, J. Mater. Res. 7 (1992) 1564–1583, doi:10.1557/JMR.1992.1564.

[36] L. Papadopoulos, N.M. Malitowski, A. Zamboulis, S. Friebel, D. Bikiaris, T. Robert, Influence of bio-based 2,5-furandicarboxylic acid on the properties of water-borne polyurethane dispersions, React. Funct. Polym. 190 (2023) 105622, doi:10.1016/j.reactfunctpolym.2023.105622.

[37] G.J. Noordzij, C.H.R.M. Wilsens, Cascade aza-Michael addition-cyclizations; toward renewable and multifunctional carboxylic acids for melt-polycondensation, Front. Chem. 7 (2019) 1–14, doi:10.3389/fchem.2019.00729.

[38] P. Mojon, J.P. Oberholzer, J.M. Meyer, U.C. Belser, Polymerization shrinkage of index and pattern acrylic resins, J. Prosthet. Dent. 64 (1990) 684–688, doi:10.1016/0022-3913(90)90296-O.

[39] N. Kladovasilakis, K. Tsongas, I. Kostavelis, D. Tzovaras, D. Tzetzis, Effective mechanical properties of additive manufactured triply periodic minimal surfaces: experimental and finite element study, Int. J. Adv. Manuf. Technol. 121 (2022) 7169–7189, doi:10.1007/s00170-022-09651-w.